The Astrophysical Journal, 757:33 (10pp), 2012 September 20 doi:10.1088/0004-637X/757/1/33

POLARIZED PARTIAL FREQUENCY REDISTRIBUTION IN SUBORDINATE LINES. II. SOLUTION OF THE TRANSFER EQUATION WITH RAYLEIGH SCATTERING

K. N. Nagendra and M. Sampoorna
Indian Institute of Astrophysics, IInd Block, Koramangala, Bangalore 560 034, India; knn@iiap.res.in, sampoorna@iiap.res.in
Received 2012 January 24; accepted 2012 July 23; published 2012 September 4

ABSTRACT

It is quite common in line formation theory to treat scattering in subordinate lines under the assumption of complete frequency redistribution (CRD). The partial frequency redistribution (PRD) in subordinate lines cannot always be approximated by CRD, especially when the polarization state of the line radiation is taken into account. Here we investigate the PRD effects in subordinate lines including scattering polarization. The line formation is described by a polarized non-LTE line transfer equation based on a two-level atom model. We use the recently derived subordinate line redistribution matrix. We devise polarized approximate lambda iteration methods to solve the concerned transfer problem. The linear polarization profiles of subordinate lines formed in non-magnetic (Rayleigh) scattering atmospheres are discussed. We consider one-dimensional isothermal planar model atmospheres. We show that in the polarized line transfer calculations of subordinate lines, PRD plays as important of a role as it does in the case of resonance lines. We also study the effect of collisions on linear polarization profiles of subordinate lines.

Key words: line: profiles – polarization – radiative transfer – scattering – Sun: atmosphere

1. INTRODUCTION

The problem of spectral line polarization by resonance scattering is well known. The mechanism responsible for generating line polarization is the Rayleigh (dipole) scattering on the atomic bound states. We confine our attention to a two-level atom model with an unpolarized lower level. If the lower level of the atom is a ground state, then the problem of partial frequency redistribution (PRD) including elastic collisions in line scattering can be represented by a combination (see Omont et al. 1972) of $R_{\rm II}$ and $R_{\rm III}$ functions of Hummer (1962). However, if the lower level is also an excited state of the atom, then the relevant PRD function to be used is a combination of $R_{\rm V}$ and $R_{\rm III}$ (Heinzel & Hubeny 1982). The $R_{\rm V}$ function describes line scattering on radiatively broadened upper and lower levels (namely, the subordinate lines). The form of the $R_{\rm V}$ function in the laboratory frame was derived by Heinzel (1981). Detailed studies of the nature of this function in angle-dependent and angle-averaged forms were presented, respectively, in Heinzel (1981) and Heinzel & Hubeny (1983; see also Frisch 1980). The angle-averaged version of this function was used in unpolarized line transfer computations by Hubeny & Heinzel (1984) and by Mohan Rao et al. (1984). It is shown that the emergent intensity profile computed with the $R_{\rm V}$ function lies between those computed with $R_{\rm II}$ and complete frequency redistribution (CRD).

Most of the polarized line transfer computations so far have been performed using the well-known redistribution functions of Hummer (1962). See Nagendra (2003) and Nagendra & Sampoorna (2009) for a review of the recent literature on the subject. The only exceptions are the papers by McKenna (1984) and Nagendra (1994, 1995) where $R_{\rm V}$ is also studied. While it is true that most of the strong lines in the solar spectrum are resonance lines (the lower level being the ground state of the atom), there are several lines that are subordinate (with a broadened lower level) and are polarized. The purpose of this paper is to revisit the problem of scattering polarization in subordinate lines arising due to transitions between two excited states. We also re-examine the traditional use of CRD for subordinate lines, instead of the actual PRD function $R_{\rm V}$.

The problem of frequency redistribution in polarized resonance scattering of radiation on two atomic levels that are broadened both radiatively and collisionally was addressed by Omont et al. (1972). Domke & Hubeny (1988) particularized the results of Omont et al. (1972) to the case of polarization. For resonance lines (infinitely sharp lower level) they derived explicit form of the laboratory frame redistribution matrix (RM). A more general formulation of the polarized RM for a two-level atom model including the effects of collisions and magnetic fields is that of Bommier (1997a, 1997b). Apart from the case of resonance lines, Bommier (1997a, 1997b) also considered the case of polarized redistribution in subordinate lines with radiatively and collisionally broadened upper and lower levels. Whereas in the case of resonance lines explicit laboratory frame RMs were derived, the corresponding expressions for the subordinate lines were not given in these two papers. Recently, Sampoorna (2012) has derived the explicit form of the laboratory frame RM for subordinate lines combining the results of Domke & Hubeny (1988) and Heinzel & Hubeny (1982). In the present paper, we use this newly derived RM for subordinate lines in the polarized line transfer computations.

In Nagendra (1994, 1995) a discrete ordinate finite difference method was used for the solution of the polarized transfer problem. The solutions were presented for self-emitting slabs of finite optical thickness and small bandwidths in frequency. The role of elastic and inelastic collisions on resonance and subordinate lines was discussed in great detail. For resonance lines, the RM derived by Domke & Hubeny (1988) was used, while for the subordinate lines a product of collisional redistribution function of Heinzel & Hubeny (1982) and Rayleigh phase matrix was used. Moreover, Nagendra (1994, 1995) used the so-called hybrid approximation, which was introduced into the polarized line transfer by Rees & Saliba (1982). It allows the RM to be replaced by a simple product of the phase matrix (that represents the angular correlations) and the traditional angle-averaged redistribution functions (that fully represent the frequency correlations).

In this paper, we use polarized approximate lambda iteration (PALI) methods to solve the polarized line transfer equation for subordinate lines. Following Rees & Saliba (1982), we use the

angle-averaged version of the subordinate line RM presented in Sampoorna (2012). We also use the azimuth-averaged subordinate line RM derived in the above-mentioned paper. The basic algorithm of the PALI method in the case of resonance lines can be found in Nagendra & Sampoorna (2009) for angle-averaged version of the RM and in Sampoorna et al. (2011) for azimuth-averaged RM. In this paper, we describe the essential generalizations required for treating subordinate line RM (in both angle-averaged and azimuth-averaged cases). We present emergent Stokes I, and fractional linear polarization Q/I profiles formed in isothermal planar slab atmospheres, specified by few model parameters. The effect of elastic collisions is also discussed.

The subordinate line RM is briefly recalled in Section 2. In Section 3 we describe the basic equations of the problem. In Section 4 we discuss the numerical method of solution. Section 5 is devoted to a study of the angle-averaged as well as the azimuth-averaged type-V redistribution function. Section 6 concerns a discussion of the results. Conclusions are presented in Section 7.

2. SUBORDINATE LINE REDISTRIBUTION MATRIX

Here we recall the explicit form of the azimuth-averaged subordinate line RM presented in Sampoorna (2012). We also present the angle-averaged analog of this RM. We use slightly different notations than those used by Sampoorna (2012) for clarity.

The elements of the azimuth-averaged RM for subordinate lines are given by

$$\mathbf{R}_{ij}(x,\mu,x',\mu') = \sum_{K=0}^{2}\sum_{Q\geqslant 0}^{K} \mathcal{F}_Q^K(x,\mu,x',\mu') \times \tilde{T}_Q^K(i,\mu)\tilde{T}_Q^K(j,\mu'), \quad (1)$$

where $i, j = 0, 1$, and

$$\mathcal{F}_Q^K = \widetilde{\mathcal{R}}_{\rm V}^{(K,Q)} + [W_K\beta^{(K)} - \delta^{(K)}]\mathcal{R}_{\rm III}^{(Q),{\rm sl}}. \quad (2)$$

In the above equation the superscript "sl" stands for subordinate line. Here x', x denote the incident and scattered frequencies in Doppler width units, and μ', μ are the direction cosines of incoming and outgoing rays, respectively. The irreducible tensors $\tilde{T}_Q^K(i,\mu)$ are defined in Frisch (2010). $W_K(J_l, J_u)$ are the K-multipole atomic polarizability factors that depend on the angular momentum of the lower (J_l) and upper (J_u) levels of the transition. The quantity $\widetilde{\mathcal{R}}_{\rm V}^{(K,Q)}$ is given by

$$\widetilde{\mathcal{R}}_{\rm V}^{(K,Q)} = \sum_{K'=0}^{2} \alpha^{(K')}\bar{C}_{KK'J_lJ_u}\mathcal{R}_{\rm V}^{(K',Q)}(x,\mu,x',\mu'). \quad (3)$$

The coefficients $\alpha^{(K)}$ and $\beta^{(K)}$ are branching ratios given by

$$\alpha^{(K)} = \frac{\Gamma_{\rm R}^{(u)}}{\Gamma_{\rm R}^{(u)} + \Gamma_{\rm I}^{(u)} + \Gamma_{\rm E} - D_l^{(K)}}, \quad (4)$$

$$\beta^{(K)} = \frac{\Gamma_{\rm R}^{(u)}}{\Gamma_{\rm R}^{(u)} + \Gamma_{\rm I}^{(u)} + D_u^{(K)}}. \quad (5)$$

Here $\Gamma_{\rm R}^{(u)}$ is the radiative transition rate of the upper level (u), $\Gamma_{\rm I}^{(u)}$ is the inelastic collisional deexcitation rate of the level u, and $\Gamma_{\rm E}$ is the elastic collisional rate for the specific transition. $D_l^{(K)}$ and $D_u^{(K)}$ are the $2K$-multipole destruction rates for levels l and u, respectively. Note that $D_l^{(0)} = D_u^{(0)} = 0$. The quantity $\delta^{(K)}$ is given by

$$\delta^{(K)} = \sum_{K'=0}^{2} \alpha^{(K')}\bar{C}_{KK'J_lJ_u}, \quad (6)$$

where

$$\bar{C}_{KK'J_lJ_u} = (-1)^{K+K'}\,3(2J_u+1)(2K'+1) \times \begin{Bmatrix} 1 & 1 & K \\ 1 & 1 & K' \end{Bmatrix} \begin{Bmatrix} 1 & 1 & K' \\ J_l & J_l & J_u \end{Bmatrix}^2. \quad (7)$$

The factors $\mathcal{R}_{\rm V}^{(K,Q)}$ and $\mathcal{R}_{\rm III}^{(Q),{\rm sl}}$ are the azimuthal Fourier coefficients of order Q of the angle-dependent (AD) PRD functions $R_{\rm V,AD}^{(K)}$ and $R_{\rm III,AD}^{\rm sl}$, respectively. They are defined by

$$\mathcal{R}_{\rm V}^{(K,Q)}(x,\mu,x',\mu') = \frac{2-\delta_{0Q}}{2\pi} \times \int_0^{2\pi} R_{\rm V,AD}^{(K)}(x,\mu,x',\mu',\Delta)\cos Q\Delta\, d\Delta, \quad (8)$$

with a similar expression for $\mathcal{R}_{\rm III}^{(Q),{\rm sl}}$. Here Δ is the azimuth difference between the scattered and incident rays. The angle-dependent function $R_{\rm V,AD}^{(K)}$ is derived in Heinzel & Hubeny (1982). They have the same functional form as their pure radiative counterpart derived in Heinzel (1981). However, the upper and lower level damping widths in the collisional redistribution case are given by

$$a_u = \frac{\Gamma_{\rm R}^{(u)} + \Gamma_{\rm I}^{(u)} + \Gamma_{\rm E}}{4\pi\Delta\nu_{\rm D}}, \quad (9)$$

$$a_l^{(K)} = \frac{\Gamma_{\rm R}^{(l)} + \Gamma_{\rm I}^{(l)} + D_l^{(K)}}{4\pi\Delta\nu_{\rm D}}, \quad (10)$$

where $\Delta\nu_{\rm D}$ is the Doppler width of the line. Here $\Gamma_{\rm R}^{(l)}$ and $\Gamma_{\rm I}^{(l)}$ are the radiative and inelastic collisional widths of the lower level l. The $R_{\rm III,AD}^{\rm sl}$ has the same functional form as that derived by Hummer (1962) for a resonance line, but the total damping width is now given by

$$a = \frac{\Gamma_{\rm R}^{(u)} + \Gamma_{\rm R}^{(l)} + \Gamma_{\rm I}^{(u)} + \Gamma_{\rm I}^{(l)} + \Gamma_{\rm E}}{4\pi\Delta\nu_{\rm D}}. \quad (11)$$

We can show that the index Q takes value zero only, when we use angle-averaged type-V and type-III functions in place of their angle-dependent counterparts (see, e.g., Frisch 2010). It also follows from our Equation (8). Thus, the angle-averaged (AA) form of Equation (1) can be written as

$$\mathbf{R}_{ij}^{\rm AA}(x,\mu,x',\mu') = \sum_{K=0}^{2} F_{\rm AA}^K(x,x')\tilde{T}_0^K(i,\mu)\tilde{T}_0^K(j,\mu'), \quad (12)$$

where

$$F_{\rm AA}^K = \tilde{R}_{\rm V,AA}^{(K)} + [W_K\beta^{(K)} - \delta^{(K)}]R_{\rm III,AA}^{\rm sl}, \quad (13)$$

with

$$\tilde{R}^{(K)}_{\rm V,AA} = \sum_{K'=0}^{2} \alpha^{(K')} \bar{C}_{KK'J_lJ_u} R^{(K')}_{\rm V,AA}(x, x'). \quad (14)$$

The angle-averaged redistribution functions are computed using

$$R^{(K)}_{\rm V,AA}(x, x') = \frac{1}{2}\int_0^{\pi} R^{(K)}_{\rm V,AD}(x, x', \Theta) \sin\Theta\, d\Theta, \quad (15)$$

with a similar expression for $R^{\rm sl}_{\rm III,AA}$. Here Θ is the scattering angle between incident and scattered rays.

We remark that for $J_l = 0$ or $1/2$ the second 6-j symbol in $\bar{C}_{KK'J_lJ_u}$ vanishes for $K' = 1$ and 2. As a result $D^{(K')}_l$ that enters $\alpha^{(K')}$ and $\mathcal{R}^{(K',Q)}_{\rm V}$ or $R^{(K')}_{\rm V,AA}$ does not make any contribution to the linear polarization. Further for J_l other than 0 and $1/2$, our numerical experiments showed that the lower level elastic collision rates $D^{(K')}_l$ again do not effect the linear polarization profiles. This is possibly because the lower level is unpolarized in the present formulation of the scattering theory used here, namely, the magnetic substates of the lower level are "assumed" to be equally populated. The elastic collisions can redistribute populations among the magnetic substates of a given level. Due to the imposition of the equality of m-state population, the $D^{(K')}_l$ rates are allowed to contribute only to maintain this equilibrium population. In this way although $D^{(K')}_l$ of the lower level are included in the present formulation, they are "ineffective" and do not produce depolarization, which would have been possible, if the lower level was allowed to be polarized.

3. GOVERNING EQUATIONS OF THE PROBLEM

We consider a one-dimensional planar slab atmosphere, without any magnetic fields. Therefore, the polarized radiation field is axisymmetric and is represented by the Stokes parameters I and Q. The positive Q direction is defined in the plane containing the direction of the ray and the atmospheric normal.

The polarized line transfer equation for the Stokes vector component can be written as

$$\mu \frac{\partial I_i}{\partial \tau} = [\varphi(x) + r][I_i(\tau, x, \mu) - S_i(\tau, x, \mu)], \quad (16)$$

where $I_i = (I, Q)$ for $i = 0, 1$; τ is the line optical depth; and r is the ratio of continuum to the frequency-integrated line absorption coefficient. The absorption profile function is a Voigt function with total damping width a given by Equation (11). The total source vector is defined as

$$S_i(\tau, x, \mu) = \frac{\varphi(x) S_{l,i}(\tau, x, \mu) + r S_{c,i}}{\varphi(x) + r}, \quad (17)$$

where $S_{c,i}$ are the unpolarized continuum source vector components, with $S_{c,0} = B_{\nu_0}$, the Planck function at the line center frequency. The line source vector can be written as

$$S_{l,i}(\tau, x, \mu) = G_i(\tau) + \int_{-\infty}^{+\infty} dx' \int_{-1}^{+1} \frac{d\mu'}{2} \sum_{j=0}^{1} \times \frac{\mathbf{R}_{ij}(x, \mu, x', \mu')}{\varphi(x)} I_j(\tau, x', \mu'). \quad (18)$$

The unpolarized primary source within the slab is $G_0(\tau) = \epsilon B_{\nu_0}$ and $G_1(\tau) = 0$, with ϵ being the thermalization parameter given by

$$\epsilon = \frac{\Gamma^{(u)}_{\rm I}}{\Gamma^{(u)}_{\rm I} + \Gamma^{(u)}_{\rm R}}. \quad (19)$$

The RM for the subordinate line $\mathbf{R}_{ij}$ is given by Equation (1) for azimuth-averaged case and by Equation (12) for the angle-averaged case.

Following Frisch (2010), we can decompose I_i into its irreducible components $\mathcal{I}^K_Q$ as

$$I_i(\tau, x, \mu) = \sum_{K=0,2} \sum_{Q\geqslant 0}^{K} \tilde{\mathcal{T}}^K_Q(i, \mu) \mathcal{I}^K_Q(\tau, x, \mu), \quad i = 0, 1, \quad (20)$$

with a similar expression for S_i, $S_{c,i}$, G_i, and $S_{l,i}$. Clearly there are four terms in the summation for azimuth-averaged case and two terms for the angle-averaged case. The irreducible line source vector components $\mathcal{S}^K_{l,Q}$ may be written as

$$\mathcal{S}^K_{l,Q}(\tau, x, \mu) = \mathcal{G}^K_Q(\tau) + \int_{-\infty}^{+\infty} dx' \int_{-1}^{+1} \frac{d\mu'}{2} \times \frac{\mathcal{F}^K_Q(x, \mu, x', \mu')}{\varphi(x)} \sum_{K'=0,2} \sum_{Q'\geqslant 0}^{K'} \tilde{\Gamma}^{KK'}_{QQ'}(\mu') \mathcal{I}^{K'}_{Q'}(\tau, x', \mu'), \quad (21)$$

where

$$\tilde{\Gamma}^{KK'}_{QQ'}(\mu') = \sum_{j=0}^{1} \tilde{\mathcal{T}}^K_Q(j, \mu') \tilde{\mathcal{T}}^{K'}_{Q'}(j, \mu'). \quad (22)$$

The explicit form of $\tilde{\Gamma}^{KK'}_{QQ'}(\mu')$ can be found in Frisch (2010). The components $\mathcal{I}^K_Q$ satisfy a transfer equation similar to Equation (16). The source term is given by Equation (17), where $S_{l,i}$ and $S_{c,i}$ are replaced by $\mathcal{S}^K_{l,Q}$ and $\mathcal{S}^K_{c,Q} = \delta_{K0}\delta_{Q0} B_{\nu_0}$. We remark that when $\mathcal{F}^K_Q$ are independent of μ and μ' (i.e., when they are replaced by $F^K_{\rm AA}$), only the $Q = 0$ components of $\mathcal{S}^K_{l,Q}$ are non-zero.

4. NUMERICAL METHOD OF SOLUTION

Here we describe the PALI method to solve the axisymmetric transfer problem for the subordinate lines in the irreducible basis. We discuss both the azimuth-averaged and angle-averaged cases. The basic steps of the PALI methods can be found in several earlier papers (see, e.g., Trujillo Bueno 2003; Nagendra & Sampoorna 2009; Sampoorna et al. 2011). Therefore we recall only the main ingredients of this method.

Define the four-component vectors $\boldsymbol{\mathcal{S}}(\tau, x, \mu) = (\mathcal{S}^0_0, \mathcal{S}^2_0, \mathcal{S}^2_1, \mathcal{S}^2_2)^{\rm T}$ and $\boldsymbol{\mathcal{I}}(\tau, x, \mu) = (\mathcal{I}^0_0, \mathcal{I}^2_0, \mathcal{I}^2_1, \mathcal{I}^2_2)^{\rm T}$. The formal solution of the transfer equation for the four-component irreducible vector $\boldsymbol{\mathcal{I}}$ can be written as

$$\boldsymbol{\mathcal{I}}_{x\mu} = \boldsymbol{\Lambda}_{x\mu}[\boldsymbol{\mathcal{S}}_{x\mu}], \quad (23)$$

where for notational brevity the dependence on x and μ appear as subscripts. $\boldsymbol{\Lambda}_{x\mu}$ is the frequency- and angle-dependent (4×4) integral operator for azimuth-averaged case. For angle-averaged case $\boldsymbol{\Lambda}$ depends only on x and is a (2×2) integral operator. The iteration method is based on the introduction of an approximate Lambda operator $\boldsymbol{\Lambda}^*_{x\mu}$, which is taken as a local operator in space (Jacobi method). At each step in the iterative process, one has current estimates of $\boldsymbol{\mathcal{S}}^{(n)}_{x\mu}$ and $\boldsymbol{\mathcal{S}}^{(n)}_{l,x\mu}$, where the superscript (n) refers to the nth iteration step. The source vector corrections

$\delta\boldsymbol{\mathcal{S}}^{(n)}_{l,x\mu}$ are given at each depth point by a system of linear equations:

$$\delta\boldsymbol{\mathcal{S}}^{(n)}_{l,x\mu} - \int_{-\infty}^{+\infty} dx' \int_{-1}^{+1} \frac{d\mu'}{2} \frac{\boldsymbol{\mathcal{F}}_{x\mu,x'\mu'}}{\varphi_x} \boldsymbol{\Gamma}_{\mu'} p_{x'} \times \boldsymbol{\Lambda}^*_{x'\mu'}\left[\delta\boldsymbol{\mathcal{S}}^{(n)}_{l,x'\mu'}\right] = \boldsymbol{\mathcal{G}}(\tau) + \overline{\boldsymbol{\mathcal{J}}}^{(n)}_{x\mu} - \boldsymbol{\mathcal{S}}^{(n)}_{l,x\mu}, \quad (24)$$

where $p_x = \varphi_x/(\varphi_x + r)$ and

$$\overline{\boldsymbol{\mathcal{J}}}^{(n)}_{x\mu} = \int_{-\infty}^{+\infty} dx' \int_{-1}^{+1} \frac{d\mu'}{2} \frac{\boldsymbol{\mathcal{F}}_{x\mu,x'\mu'}}{\varphi_x} \boldsymbol{\Gamma}_{\mu'} \boldsymbol{\Lambda}_{x'\mu'}\left[\boldsymbol{\mathcal{S}}^{(n)}_{x'\mu'}\right]. \quad (25)$$

Here $\boldsymbol{\mathcal{G}}(\tau) = [G_0(\tau), 0, 0, 0]^{\mathrm{T}}$, and $\boldsymbol{\Gamma}_\mu$ is a (4×4) full matrix with elements $\tilde{\Gamma}^{KK'}_{QQ'}$ (see Equation (22)). The (4×4) matrix $\boldsymbol{\mathcal{F}}$ is diagonal, i.e., $\boldsymbol{\mathcal{F}} = \mathrm{diag}[\mathcal{F}^0_0, \mathcal{F}^2_0, \mathcal{F}^2_1, \mathcal{F}^2_2]$. Its elements are given by Equation (2) for the azimuth-averaged case. For the angle-averaged case $\boldsymbol{\mathcal{F}}$ depends only on (x, x') and K, and will be denoted by $\boldsymbol{F}_{\mathrm{AA}}$. It is now a (2×2) matrix with its diagonal elements F^K_{AA} given by Equation (13).

4.1. A Matrix Method for Subordinate lines

Equation (24) can be formally written as

$$\mathbf{A}\,\delta\boldsymbol{\mathcal{S}}^{(n)}_l = \boldsymbol{r}^{(n)}, \quad (26)$$

where the residual vector $\boldsymbol{r}^{(n)}$ is given by the right-hand side of Equation (24). For the azimuth-averaged case, at each depth point, $\boldsymbol{r}^{(n)}$ and $\delta\boldsymbol{\mathcal{S}}^{(n)}_l$ are vectors of length $4N_x\,2N_\mu$, where N_x is the number of frequency points in the range $[0, x_{\max}]$ and N_μ is the number of angle points in the range $[0 < \mu \leqslant 1]$. The matrix $\mathbf{A}$ then has the dimensions of $(4N_x\,2N_\mu \times 4N_x\,2N_\mu)$. On the other hand, for the angle-averaged case, at each depth point, $\boldsymbol{r}^{(n)}$ and $\delta\boldsymbol{\mathcal{S}}^{(n)}_l$ are vectors of length $2N_x$, and $\mathbf{A}$ is a $(2N_x \times 2N_x)$ matrix. This "matrix method" of computing $\delta\boldsymbol{\mathcal{S}}^{(n)}_l$ is referred to as frequency-angle by frequency-angle method for azimuth-averaged case (see Sampoorna et al. 2011) and as frequency-by-frequency method for angle-averaged case (see Paletou & Auer 1995; Sampoorna et al. 2008).

4.2. A Core–Wing Separation Method for Subordinate Lines

In the case of resonance lines, a core–wing method was introduced by Paletou & Auer (1995) for the computation of the line source vector corrections. This method amounts to computing the integral over frequency (see Equation (24)) separately in the core and in the wings, thereby avoiding the computationally expensive matrix inversion involved in the matrix method described above. The core–wing technique as applied to $R_{\mathrm{II,AA}}(x, x')$ function involves the assumption of CRD in the line core $(x, x') \leqslant 3$ and pure coherent scattering in the line wings $(x = x') > 3$. Such a core–wing division was introduced by Paletou & Auer (1995) based on the physical nature of the $R_{\mathrm{II,AA}}(x, x')$ function. We find that the same core–wing technique can be applied to the type-V function only when $a^{(K)}_l < a_u$. Because in this case the type-V function behaves similar to the type-II function (see Heinzel 1981; Heinzel & Hubeny 1983, and Section 5 below).

For $a^{(K)}_l \geqslant a_u$, the core–wing technique is not applicable to the type-V function. This is because, for a incident wing photon at x', the type-V function exhibits a "simultaneous" reemission probability at $x = x'$ and at $x = 0$, unlike the case of type-II function (see, e.g., Frisch 1980). Further, the peak at $x = 0$ dominates over that at $x = x'$ when $a^{(K)}_l > a_u$. In such situations (i.e., $a^{(K)}_l \geqslant a_u$), we found that using CRD function throughout the frequency range instead of type-V function provides a faster and reliable method of solution. Thus in Equation (24) (see also Equations (2) and (13)), we approximate

$$\frac{\mathcal{R}^{(K,Q)}_{\mathrm{V}}}{\varphi_x} \simeq \delta_{Q0} \begin{cases} \varphi_{x'}, & \text{for } x \leqslant x_c \text{ when } a^{(K)}_l < a_u, \\ \delta(x - x'), & \text{for } x > x_c \text{ when } a^{(K)}_l < a_u, \\ \varphi_{x'}, & \text{for all } x \text{ when } a^{(K)}_l \geqslant a_u, \end{cases} \quad (27)$$

for all values of K and

$$\frac{\mathcal{R}^{(Q),\mathrm{sl}}_{\mathrm{III}}}{\varphi_x} \simeq \delta_{Q0} \begin{cases} \varphi_{x'}, & \text{for } x \leqslant x_c, \\ 0, & \text{for } x > x_c, \end{cases} \quad (28)$$

where x_c denotes the core–wing separation frequency, usually taken as three Doppler widths. With this approximation $\boldsymbol{\mathcal{F}}$ takes the form

$$\boldsymbol{\mathcal{F}}_{x\mu,x'\mu'} \approx \varphi_x \varphi_{x'} \mathbf{W}\boldsymbol{\mathcal{B}}\boldsymbol{\mathcal{E}}, \quad (29)$$

in the core, and in the wings

$$\boldsymbol{\mathcal{F}}_{x\mu,x'\mu'} \approx \varphi_x \delta(x - x')\boldsymbol{\delta}\boldsymbol{\mathcal{E}}, \quad (30)$$

where $\mathbf{W}$, $\boldsymbol{\mathcal{B}}$, $\boldsymbol{\delta}$, and $\boldsymbol{\mathcal{E}}$ are (4×4) diagonal matrices defined by

$$\mathbf{W} = \mathrm{diag}[W_0, W_2, W_2, W_2], \quad (31)$$

$$\boldsymbol{\mathcal{B}} = \mathrm{diag}[\beta^{(0)}, \beta^{(2)}, \beta^{(2)}, \beta^{(2)}], \quad (32)$$

$$\boldsymbol{\delta} = \mathrm{diag}[\delta^{(0)}, \delta^{(2)}, \delta^{(2)}, \delta^{(2)}], \quad (33)$$

$$\boldsymbol{\mathcal{E}} = \mathrm{diag}[1, 1, 0, 0]. \quad (34)$$

Substituting Equations (29) and (30) into Equation (24), we obtain after simple algebra

$$\delta\boldsymbol{\mathcal{S}}^{(n)}_{l,x\mu} = \boldsymbol{r}^{(n)}_{x\mu} + (1 - \alpha_x)\mathbf{W}\boldsymbol{\mathcal{B}}\boldsymbol{\mathcal{E}}\boldsymbol{\Delta T}^{\mathrm{core}} + \alpha_x \boldsymbol{\delta}\boldsymbol{\mathcal{E}}\boldsymbol{\Delta T}^{\mathrm{wing}}_x, \quad (35)$$

where α_x is the core–wing separation coefficient. In the core $\alpha_x = 0$ and in the wings $\alpha_x = R^{(0)}_{\mathrm{V,AA}}(x, x)/\varphi(x)$. The frequency and angle-independent four-dimensional vector $\boldsymbol{\Delta T}^{\mathrm{core}}$ is given by

$$\boldsymbol{\Delta T}^{\mathrm{core}} = \int_{-x_c}^{+x_c} \varphi_{x'} dx' \int_{-1}^{+1} \frac{d\mu'}{2} p_{x'} \boldsymbol{\Gamma}_{\mu'} \boldsymbol{\Lambda}^*_{x'\mu'}\left[\delta\boldsymbol{\mathcal{S}}^{(n)}_{l,x'\mu'}\right], \quad (36)$$

and the frequency-dependent but angle-independent vector $\boldsymbol{\Delta T}^{\mathrm{wing}}_x$ is given by

$$\boldsymbol{\Delta T}^{\mathrm{wing}}_x = \int_{-1}^{+1} \frac{d\mu'}{2} p_x \boldsymbol{\Gamma}_{\mu'} \boldsymbol{\Lambda}^*_{x\mu'}\left[\delta\boldsymbol{\mathcal{S}}^{(n)}_{l,x\mu'}\right]. \quad (37)$$

Following the standard procedure (see, e.g., Sampoorna et al. 2011), the final expression for $\boldsymbol{\Delta T}^{\mathrm{core}}$ is given by

$$\boldsymbol{\Delta T}^{\mathrm{core}} = \left[\mathbf{E} - \left(\int_{-x_c}^{+x_c} \varphi_x dx \int_{-1}^{+1} \frac{d\mu}{2} p_x \boldsymbol{\Gamma}_\mu \boldsymbol{\Lambda}^*_{x\mu}\right) \mathbf{W}\boldsymbol{\mathcal{B}}\boldsymbol{\mathcal{E}}\right]^{-1} \overline{\boldsymbol{r}}^{(n)}, \quad (38)$$

where $\mathbf{E}$ is a (4×4) unity matrix and

$$\bar{\boldsymbol{r}}^{(n)} = \int_{-x_c}^{+x_c} \varphi_x dx \int_{-1}^{+1} \frac{d\mu}{2} p_x \boldsymbol{\Gamma}_\mu \boldsymbol{\Lambda}^*_{x\mu} \left[\boldsymbol{r}^{(n)}_{x\mu}\right]. \quad (39)$$

Similarly, the final expression for $\boldsymbol{\Delta T}_x^{\rm wing}$ is given by

$$\boldsymbol{\Delta T}_x^{\rm wing} = \left[\mathbf{E} - \alpha_x \left(\int_{-1}^{+1} \frac{d\mu}{2} p_x \boldsymbol{\Gamma}_\mu \boldsymbol{\Lambda}^*_{x\mu}\right) \boldsymbol{\delta\mathcal{E}}\right]^{-1} \times \left[\tilde{\boldsymbol{r}}_x^{(n)} + (1-\alpha_x)\left(\int_{-1}^{+1} \frac{d\mu}{2} p_x \boldsymbol{\Gamma}_\mu \boldsymbol{\Lambda}^*_{x\mu}\right) \times \mathbf{W}\boldsymbol{\mathcal{B}\mathcal{E}}\, \boldsymbol{\Delta T}^{\rm core}\right], \quad (40)$$

where

$$\tilde{\boldsymbol{r}}_x^{(n)} = \int_{-1}^{+1} \frac{d\mu}{2} p_x \boldsymbol{\Gamma}_\mu \boldsymbol{\Lambda}^*_{x\mu} \left[\boldsymbol{r}^{(n)}_{x\mu}\right]. \quad (41)$$

We remark that when $a_l^{(K)} \geqslant a_u$, we replace x_c by $x_{\rm max}$ (or ∞) and set $\alpha_x = 0$ for all x, so that the term with $\boldsymbol{\Delta T}_x^{\rm wing}$ in Equation (35) does not contribute to $\delta\boldsymbol{\mathcal{S}}^{(n)}_{l,x\mu}$. Such a method to evaluate $\delta\boldsymbol{\mathcal{S}}^{(n)}_{l,x\mu}$ is similar to that proposed by Scharmer (1983) for $R_{\rm II,AA}$ function (and referred to as the CRDA method by Paletou & Auer 1995). It may be recalled that the CRDA method fails when applied to the $R_{\rm II,AA}$ function as demonstrated by Paletou & Auer (1995). We have verified that the core–wing separation method (applicable to $a_l^{(K)} < a_u$) and the CRDA method (applicable to $a_l^{(K)} \geqslant a_u$) for subordinate lines give exactly the same solution as that obtained by using the matrix method. While the matrix method is computationally slower and requires larger memory, the core–wing and CRDA methods are much faster since the computation of $\delta\boldsymbol{\mathcal{S}}^{(n)}_{l,x\mu}$ is analytically reduced to simple algebraic operations.

5. THE TYPE-V REDISTRIBUTION FUNCTION

Here we study the nature of type-V redistribution function for pure radiatively broadened upper and lower levels. We consider both the angle-averaged and azimuth-averaged cases. The $R^{(K)}_{\rm V,AA}$, $R^{(K)}_{\rm V,AD}$, and $\mathcal{R}^{(K,Q)}_{\rm V}$ are independent of K when both the upper and lower levels are only radiatively broadened. In this case, the upper and lower level radiative widths are given by

$$a_{l,\rm R} = \frac{\Gamma^{(l)}_{\rm R}}{4\pi\Delta\nu_{\rm D}}; \quad a_{u,\rm R} = \frac{\Gamma^{(u)}_{\rm R}}{4\pi\Delta\nu_{\rm D}}. \quad (42)$$

Thus in this section we drop the index K on the type-V function.

The nature of the type-V redistribution function for both angle-dependent and angle-averaged cases were presented in Heinzel (1981) and Heinzel & Hubeny (1983; see also Frisch 1980). The $R_{\rm V,AD}$ function consists of two terms, namely, the main term and the $E_{\rm V}$ term (see, e.g., Equation (18) of Nagendra 1994). The main term is simply a product of two Voigt functions, while the $E_{\rm V}$ term contains an integral. The $E_{\rm V}$ term has to be computed with high accuracy because it can take both positive and negative values (see Figure 4 of Heinzel 1981), which then either adds or subtracts with the main term. Inaccurate computation of the $E_{\rm V}$ term can lead to negative values of the $R_{\rm V,AD}$ function, which in turn affects the normalization of the type-V function. Heinzel (1981) and Heinzel & Hubeny (1983) have developed quadrature methods for accurate evaluation of the $E_{\rm V}$ term. Following Nagendra (1994), we use a Simpson's (1/3)rd rule with very fine grid points to evaluate the $E_{\rm V}$ term. The evaluation of the $E_{\rm V}$ term forms the main part of the computing efforts.

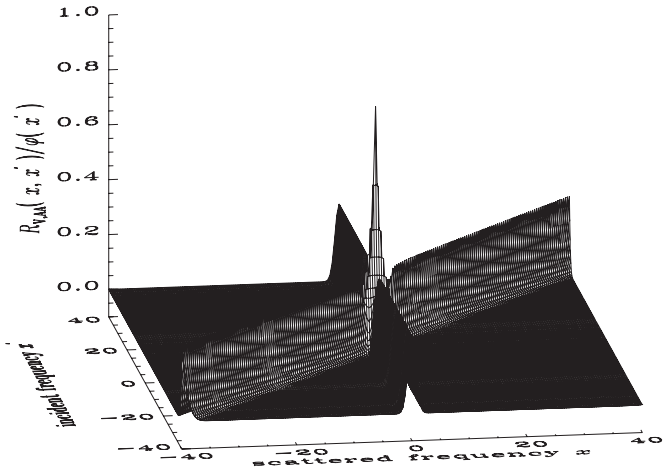

Figure 1. Probability of reemission at scattered frequency x, for absorption at the incident frequency x', in the case of angle-averaged redistribution function $R_{\rm V,AA}$. The damping parameters $a_{l,\rm R} = a_{u,\rm R} = 10^{-3}$.

5.1. Angle-averaged Case

Figure 1 displays the reemission probability $R_{\rm V,AA}(x, x')/\varphi(x')$ in the form of a surface plot for $a_{l,\rm R} = a_{u,\rm R} = 10^{-3}$. Clearly, for absorption in the wings ($x' > 3$), there is a joint probability of reemission at the line center ($x = 0$) and at $x = x'$. Further, these two peaks are of equal amplitude (because $a_{l,\rm R} = a_{u,\rm R}$) and are of constant heights outside the Doppler-core region. The latter behavior of wing coherent peak is analogous to the angle-averaged type-II function, while that of central peak is analogous to the angle-averaged type-III function. As $a_{u,\rm R}$ increases compared with $a_{l,\rm R}$, the coherent wing peak becomes more and more important, so that for $a_{u,\rm R} \gg a_{l,\rm R}$ the type-V function approaches the type-II function. On the other hand, when $a_{l,\rm R}$ increases compared with $a_{u,\rm R}$, the central peak gains importance and eventually for $a_{u,\rm R} \ll a_{l,\rm R}$ one arrives at the type-III function (see Heinzel & Hubeny 1983, for a detailed discussion).

5.2. Azimuth-averaged Case

Figure 2 shows $\mathcal{R}^{(Q)}_{\rm V}(x, \mu, x', \mu')/\varphi(x')$ versus outgoing frequency x for $\mu = 0.1$ and $\mu' = 0.9$ and for different values of incoming frequency x'. As in the case of type-II and type-III azimuthal Fourier coefficients, the $Q = 0$ coefficient of the type-V function (namely $\mathcal{R}^{(0)}_{\rm V}$) should be normalized to the absorption profile when integrated over all the incoming frequencies and angles, while $\mathcal{R}^{(Q)}_{\rm V}$ with $Q = 1, 2$ should be normalized to zero. This is necessary to ensure accurate evaluation of intensity and linear polarization profiles. The details of numerical evaluation of azimuthal Fourier coefficients of type II and type III are discussed in Sampoorna et al. (2011). We use the same method for computing the azimuthal Fourier coefficient of the type-V function.

The $\mathcal{R}^{(Q)}_{\rm V}/\varphi(x')$ decreases with increasing azimuthal order Q. This is in accordance with the behavior of the corresponding type-II and type-III cases (see, e.g., Domke & Hubeny 1988; Sampoorna et al. 2011; Nagendra & Sampoorna 2011). Similar to the angle-averaged type-V redistribution function, the

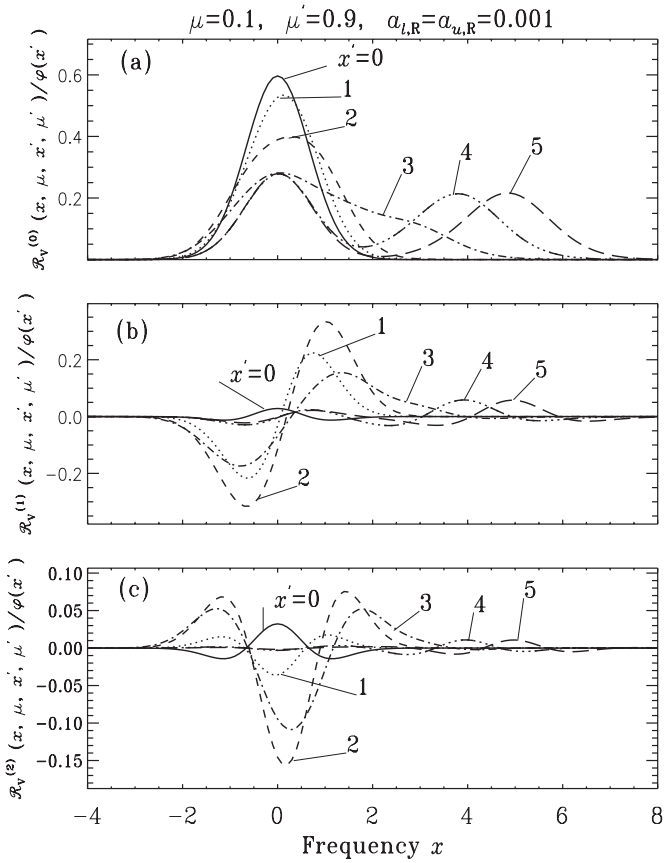

Figure 2. Azimuth-averaged type-V redistribution function vs. outgoing frequency x for $\mu = 0.1$, $\mu' = 0.9$, and $a_{l,\mathrm{R}} = a_{u,\mathrm{R}} = 0.001$. Panel (a) corresponds to $Q = 0$, panel (b) to $Q = 1$, and panel (c) to $Q = 2$. Different line types represent different incoming frequencies x'.

$\mathcal{R}_{\mathrm{V}}^{(0)}/\varphi(x')$ exhibits double maxima for incoming frequencies in the wings. For incoming frequencies in the line core ($x' < 3$), $\mathcal{R}_{\mathrm{V}}^{(Q)}/\varphi(x')$ has a behavior quite similar to the corresponding type-II function, but considerable differences occur for $x' \geqslant 3$. This occurs because of the differences between the type-II and type-V functions, which are described in Section 5.1.

6. RESULTS AND DISCUSSIONS

We present the polarization profiles emerging from isothermal constant property media. In Sections 6.2–6.4, we consider the angle-averaged version of the RM (see Equations (12)–(15)). A comparison of emergent linear polarization profiles computed with angle-averaged and azimuth-averaged RM is presented in Section 6.5.

6.1. The Model Parameterization

We consider isothermal, plane-parallel model atmospheres characterized by (T, ϵ, r, $a_{l,\mathrm{R}}$, $a_{u,\mathrm{R}}$, $\Gamma_{\mathrm{E}}/\Gamma_{\mathrm{R}}^{(u)}$), where T is the optical thickness of the slab. We neglect the inelastic collisional width ($\Gamma_{\mathrm{I}}^{(l)}$) of the lower level. The upper and lower level radiative widths are given by Equation (42). The total damping widths of the upper and lower levels can then be computed using Equations (9) and (10). We consider a $0 \rightarrow 1 \rightarrow 0$ scattering transition for simplicity. In this case, only $D_u^{(K)}$ are operative (see the discussion at the end of Section 2). Thus, the type-V function does not depend on K, and hence we drop the index K on $R_{\mathrm{V,AA}}$ and $\mathcal{R}_{\mathrm{V}}^{(Q)}$. We assume that $D_u^{(2)} = 0.5\,\Gamma_{\mathrm{E}}$ (see, e.g., Stenflo 1994). The Planck function at the line center B_{ν_0} is taken as unity. A logarithmic depth grid with six points per decade is used, with the first depth point at $\tau_1 = 10^{-4}$. For all figures presented in Sections 6.2–6.4, the slab thickness $T = 2 \times 10^8$. A non-uniform Simpson frequency quadrature is used for evaluating frequency integrals. This quadrature is constructed in such a way that the frequency points are equally spaced in the line core and logarithmically spaced in the wings. Furthermore, the maximum frequency $x_{\max}$ is chosen such that the condition $\varphi(x_{\max})T \ll 1$ is satisfied. We have about 75 points in the interval $[0, x_{\max}]$. We use a five-point Gaussian quadrature in $[0 < \mu \leqslant 1]$.

The frequency quadrature mentioned above is sufficiently accurate for line transfer computations. However, the evaluation of the redistribution weights is done on a much finer frequency grid, consisting of several hundred points. Such a fine grid is constructed by further subdividing each frequency interval into a fine mesh of Simpson quadrature points (e.g., 41-points in each interval). This reconstruction of the frequency quadrature weights helps to ensure high accuracy in the evaluation of redistribution integrals. This procedure is somewhat similar to that of the well-known method of Adams et al. (1971). Further, the evaluation of the type-V function is numerically expensive compared with the type-II and type-III functions because of the need to compute the E_{V} term to a high accuracy (see Section 5).

6.2. A Comparison of Lines Formed Under Different Redistribution Mechanisms

Figure 3 shows a comparison of emergent Stokes profiles formed with different redistribution mechanisms. The elastic collisions are neglected (i.e., $\Gamma_{\mathrm{E}}/\Gamma_{\mathrm{R}}^{(u)} = 0$). In the intensity profile the type-III and CRD mechanisms are indistinguishable. However, in the Q/I profile they differ only in the width of the central peak (see the inset panel in Figure 3), which is larger for type III than for CRD. The type-II redistribution exhibits the characteristic intensity and Q/I profiles. Indeed, in the wings the maximum linear polarization is produced for the type-II PRD mechanism. The $R_{\mathrm{V,AA}}$ function shows slight departure from CRD only in the line core of the intensity profile. This is in agreement with the results obtained by Hubeny & Heinzel (1984). Thus, we confirm their conclusion that for intensity profiles formed in semi-infinite like atmospheres, CRD is a reasonable approximation to $R_{\mathrm{V,AA}}$. This is expected because for a photon absorbed in the wings the type-V redistribution exhibits a finite probability of reemission in the line core. Therefore, in type-V scattering PRD effects never develop to be as large as in the type-II case. The physical reasons why departures from CRD are larger for $R_{\mathrm{II,AA}}$ than for $R_{\mathrm{V,AA}}$ are described in greater detail by Hubeny (1985).

On the other hand, the Q/I profiles computed using $R_{\mathrm{V,AA}}$ and CRD differ significantly throughout the line profile. In the line core all redistribution mechanisms except CRD nearly match. In the near and far wings the Q/I profile computed using the $R_{\mathrm{V,AA}}$ redistribution differs significantly from that computed using the $R_{\mathrm{II,AA}}$ function. From Figure 3 it can be seen that CRD cannot be used in place of $R_{\mathrm{V,AA}}$ function because the Q/I profile computed with $R_{\mathrm{V,AA}}$ departs very significantly from that computed using CRD throughout the line profile (except at the line center).

6.3. Effect of Variation of Radiative Damping Rates of the Lower and Upper Levels

Figure 4 shows the sensitivity of the polarization profiles formed with the type-V redistribution mechanism to the

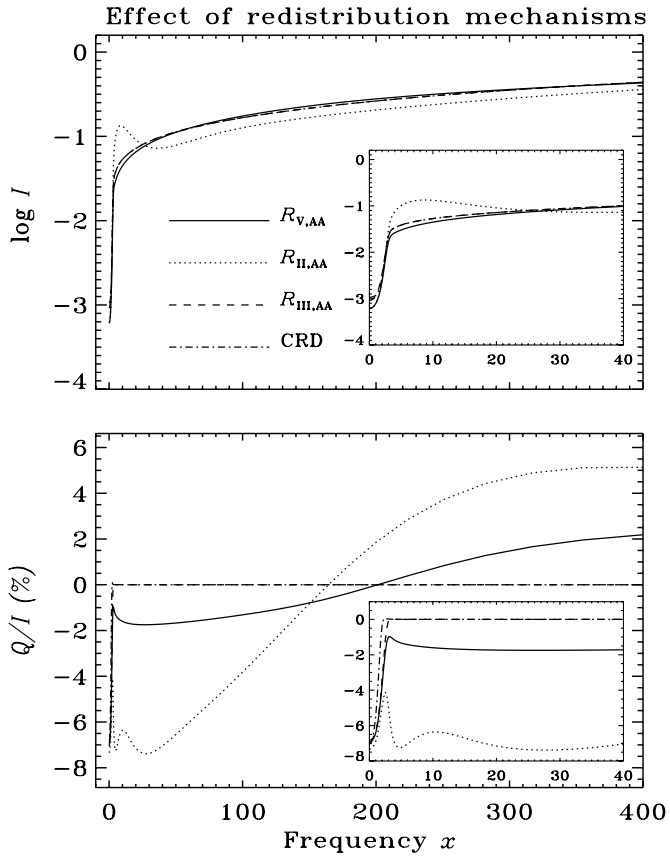

Figure 3. Comparison of emergent polarization profiles formed under different redistribution mechanisms. An isothermal atmosphere with parameters $(T,\ \epsilon,\ r,\ a_{l,\mathrm{R}},\ a_{u,\mathrm{R}},\ \Gamma_{\mathrm{E}}/\Gamma_{\mathrm{R}}^{(u)}) = (2\times10^{8},\ 10^{-6},\ 10^{-9},\ 10^{-3},\ 10^{-3},\ 0)$ is used. The line of sight is represented by $\mu = 0.05$. Different line types are solid ($R_{\mathrm{V,AA}}$), dotted ($R_{\mathrm{II,AA}}$), dashed ($R_{\mathrm{III,AA}}$), and dot-dashed (CRD). For redistribution mechanisms other than type V, a total damping width of 2×10^{-3} is used. See Section 6.2 for details.

variations in the radiative damping rates of the lower (panel a) and upper (panel b) levels. For comparison, we also show the corresponding Stokes profiles computed using CRD and $R_{\mathrm{II,AA}}$ redistribution mechanisms with the total damping width of $a = a_{l,\mathrm{R}} + a_{u,\mathrm{R}}$. This comparison is not shown for the case of $a_{l,\mathrm{R}} = a_{u,\mathrm{R}}$ because it is already presented in Figure 3. Again it is easy to see from Figure 4 that intensity profiles computed with $R_{\mathrm{V,AA}}$ resemble closely the CRD profiles than those computed with $R_{\mathrm{II,AA}}$.

In Figure 4(a), we vary the lower level damping width $a_{l,\mathrm{R}}$ keeping the upper level damping width $a_{u,\mathrm{R}}$ a constant. The intensity profile computed using $R_{\mathrm{V,AA}}$ becomes broader in the wings and slightly shallower in the line core with an increase in $a_{l,\mathrm{R}}$. Similar effects are seen in the intensity profiles computed with CRD. Whereas only broadening in the wings is seen in the intensity profile computed with $R_{\mathrm{II,AA}}$. The linear polarization (Q/I) computed using $R_{\mathrm{V,AA}}$ decreases in magnitude throughout the line profile, as the value of $a_{l,\mathrm{R}}$ increases. Indeed the shape of the Q/I profile changes from PRD-like to CRD-like frequency dependence (see the inset in Figure 4(a)). However, in the case of Q/I computed with $R_{\mathrm{II,AA}}$, the far wing peak is greatly shifted to larger frequencies as the value of total damping width a increases.

In Figure 4(b), we vary the upper level damping width $a_{u,\mathrm{R}}$ for a given value of $a_{l,\mathrm{R}}$. With an increase in $a_{u,\mathrm{R}}$ the intensity profile computed using $R_{\mathrm{V,AA}}$ broadens and deepens at the line center, exhibiting highly extended wings. In the Q/I profile computed with $R_{\mathrm{V,AA}}$, the line core ($x < 3$) is insensitive to variations in $a_{u,\mathrm{R}}$, but the line wing polarization is very sensitive. In particular, the magnitude of Q/I in the wings increases sharply essentially due to an increased role of coherent scattering throughout the line wings. Furthermore, with an increase in $a_{u,\mathrm{R}}$ the "frequency position of the far wing maxima" in Q/I shifts away from the line center. Finally, when $a_{u,\mathrm{R}}$ becomes larger than $a_{l,\mathrm{R}}$ the shape of the Q/I profile computed with $R_{\mathrm{V,AA}}$ start to resemble the corresponding profile computed using $R_{\mathrm{II,AA}}$ function. This is expected because the $R_{\mathrm{V,AA}}$ function approaches the $R_{\mathrm{II,AA}}$ function for $a_{u,\mathrm{R}} \gg a_{l,\mathrm{R}}$.

It is interesting to note that the PRD mechanism in both $R_{\mathrm{II,AA}}$ and $R_{\mathrm{V,AA}}$ (when $a_{u,\mathrm{R}} \geqslant a_{l,\mathrm{R}}$) exhibit "double maxima" in the Q/I profile, one in the near wing ($|x| \lesssim 20$) and the other in the distant wings ($|x| > 200$), apart from the line center peak. Whereas the line center and the inner wing peaks survive the radiative transfer effects in calculations with realistic model atmospheres, the far wing peak often vanishes due to the dominance of unpolarized continuum radiation field at those frequencies.

6.4. Effect of Variation of Elastic Collisions

Here we vary $\Gamma_{\mathrm{E}}/\Gamma_{\mathrm{R}}^{(u)}$ to study its influence on the emergent Stokes profiles, which are shown in Figure 5(a). The elastic collision rate is varied such that we cover the entire range from pure type-V scattering ($\Gamma_{\mathrm{E}}/\Gamma_{\mathrm{R}}^{(u)} = 0$) to nearly pure type-III scattering ($\Gamma_{\mathrm{E}}/\Gamma_{\mathrm{R}}^{(u)} = 10$), along with the intermediate range of nearly equal mix of type-V and type-III scattering ($\Gamma_{\mathrm{E}}/\Gamma_{\mathrm{R}}^{(u)} = 1$). As for the resonance lines, the intensity profiles for subordinate lines show considerable sensitivity to $\Gamma_{\mathrm{E}}/\Gamma_{\mathrm{R}}^{(u)}$ in the line wings. The linear polarization Q/I decreases throughout the line profile with increasing values of $\Gamma_{\mathrm{E}}/\Gamma_{\mathrm{R}}^{(u)}$, finally approaching small values for $\Gamma_{\mathrm{E}}/\Gamma_{\mathrm{R}}^{(u)} = 10$. As in the case of resonance lines (see, e.g., Nagendra 1994) $D_u^{(2)}$ mainly operates in the line core, while $\Gamma_{\mathrm{E}}/\Gamma_{\mathrm{R}}^{(u)}$ operates in the line wings.

In Figure 5(b), we compare (I, Q/I) profiles computed for subordinate lines, resonance lines, and CRD for $\Gamma_{\mathrm{E}}/\Gamma_{\mathrm{R}}^{(u)} = 1$ and 10. The intensity profiles for all the three redistribution mechanisms nearly coincide when elastic collisions are included. With an increase in $\Gamma_{\mathrm{E}}/\Gamma_{\mathrm{R}}^{(u)}$, the shape of the Q/I profile of the subordinate line resembles more closely that of the resonance line. Finally, for $\Gamma_{\mathrm{E}}/\Gamma_{\mathrm{R}}^{(u)} \geqslant 5$ both the profiles coincide and approach a CRD-like profile shape.

6.5. Comparison of Stokes Profiles Computed Using Angle-averaged and Azimuth-averaged PRD Functions

It is a common practice in most of the line transfer computations to use angle-averaged functions. It stems from the fact that angle-averaged functions indeed represent the physics of line scattering to a significant degree of realism, at least in the absence of magnetic fields. The other reasons for the use of angle-averaged functions are the drastically smaller effort in computing them and subsequently their use in the transfer equation.

In the case of resonance lines, it was shown in Sampoorna et al. (2011, see also Faurobert 1987; Nagendra et al. 2002) and Nagendra & Sampoorna (2011) that the differences between angle-averaged and angle-dependent (represented by

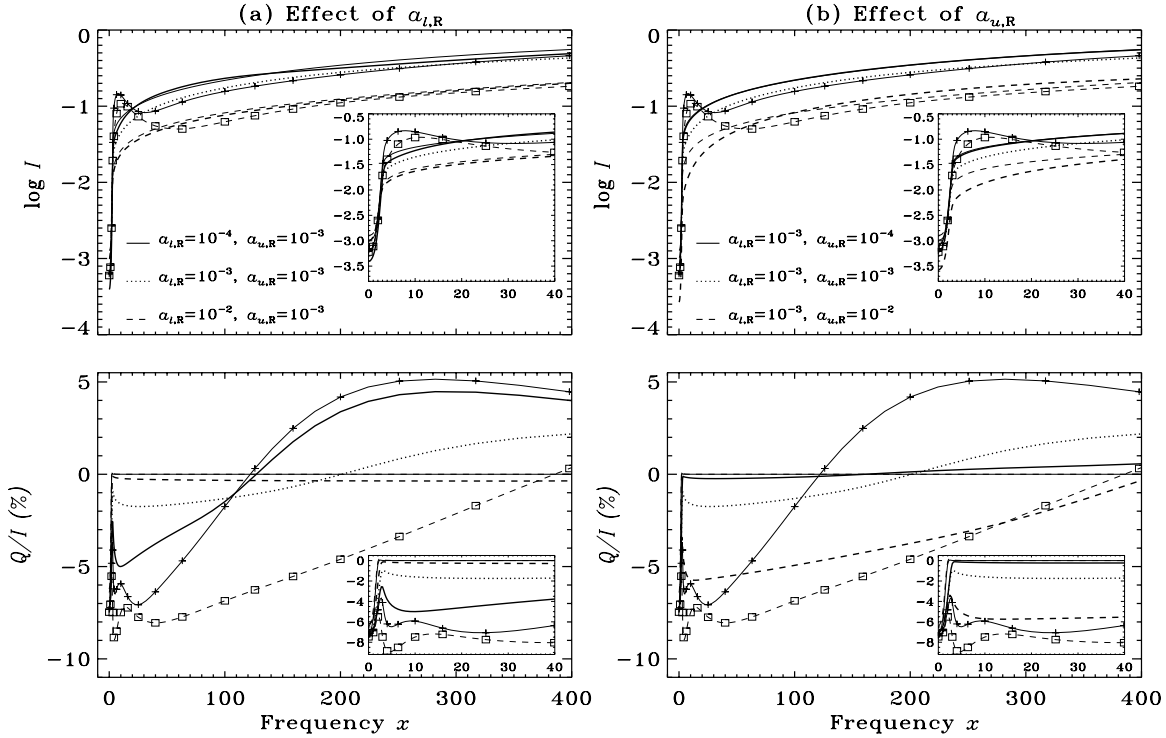

Figure 4. Effect of variation of $a_{l,\mathrm{R}}$ (a) and $a_{u,\mathrm{R}}$ (b) on the emergent polarization profiles computed in an isothermal atmosphere using type-V redistribution mechanism. Model parameters are the same as in Figure 3. Different line types are specified in each of the panels. Heavy lines without any symbols correspond to $R_{\mathrm{V,AA}}$. Thin lines without any symbol correspond to CRD and thin lines with symbols correspond to $R_{\mathrm{II,AA}}$. See Section 6.3 for details.

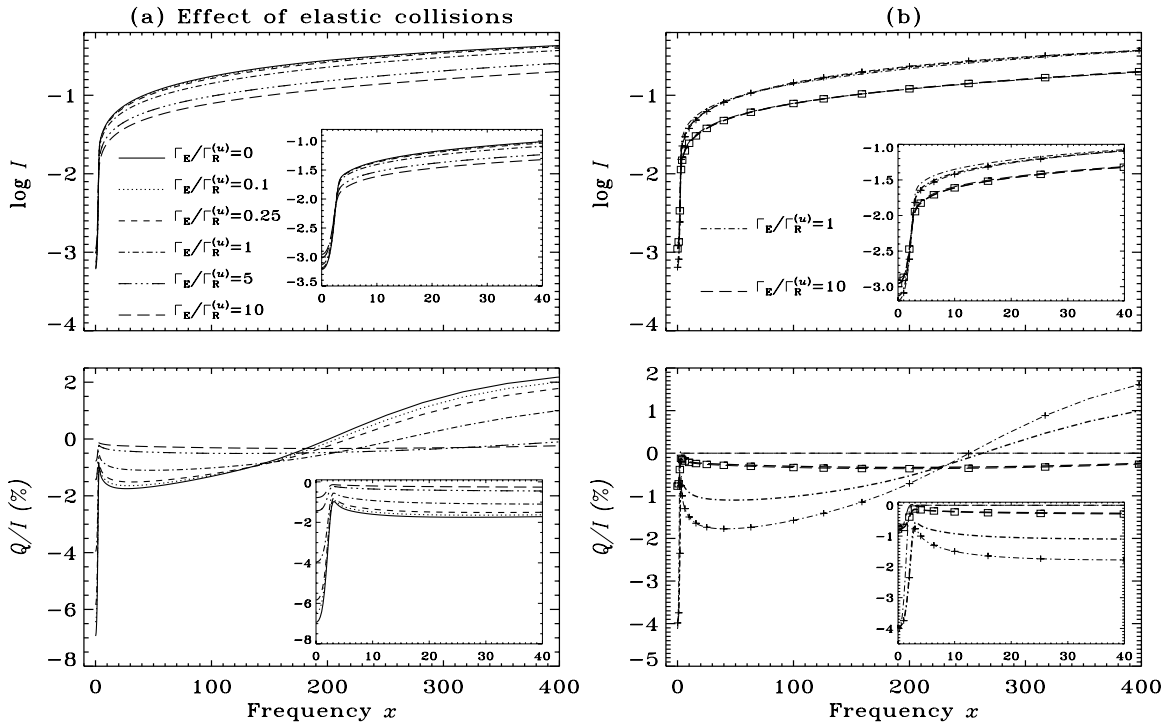

Figure 5. Panel (a) shows the effect of variation of elastic collision rate on the emergent polarization profiles of subordinate lines formed in an isothermal atmosphere. Different line types are specified in the figure. Panel (b) shows a comparison of $(I,\ Q/I)$ profiles computed with $(R_{\mathrm{V,AA}},\ R_{\mathrm{III,AA}})$, $(R_{\mathrm{II,AA}},\ R_{\mathrm{III,AA}})$ combinations, and CRD for $\Gamma_{\mathrm{E}}/\Gamma_{\mathrm{R}}^{(u)} = 1$ and 10. Heavy lines correspond to subordinate lines and thin lines without any symbols correspond to CRD, while thin lines with symbols correspond to resonance lines. Model parameters are the same as in Figure 3. See Section 6.4 for details.

azimuth-averaged RM in the case of one-dimensional planar atmospheres) results in Q/I are between 10% and 30%, particularly for slabs of smaller optical thickness. For slabs of larger optical thickness, the differences are even smaller. We find that similar conclusions hold in the case of subordinate lines also. Figure 6 illustrates this fact through a comparison of $(I,\ Q/I)$ profiles computed using angle-averaged and azimuth-averaged (basically angle-dependent) functions for an isothermal

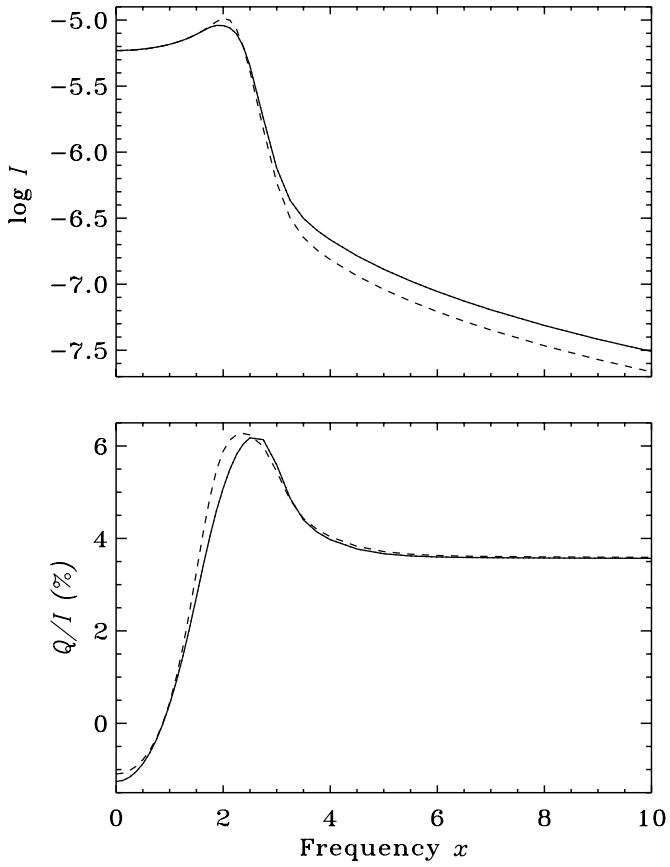

Figure 6. Comparison of emergent Stokes profiles of subordinate lines formed in an isothermal slab atmosphere, at $\mu = 0.05$ for azimuth-averaged (solid lines) and the angle-averaged (dashed lines) PRD functions. Model parameters are (T, ϵ, r, $a_{l,\mathrm{R}}$, $a_{u,\mathrm{R}}$, $\Gamma_\mathrm{E}/\Gamma_\mathrm{R}^{(u)}$) = (20, 10^{-6}, 0, 10^{-3}, 10^{-3}, 0). See Section 6.5 for details.

self-emitting slab of optical thickness $T = 20$. The elastic collisions are neglected ($\Gamma_\mathrm{E}/\Gamma_\mathrm{R}^{(u)} = 0$). Since the effects of elastic collisions on the polarization of subordinate line are identical to those on the resonance line polarization (see Section 6.4), the influence of elastic collisions on the difference between angle-averaged and azimuth-averaged solutions for subordinate lines is similar to that for the resonance lines.

7. CONCLUSIONS

In this paper, we have discussed the PRD effects in the subordinate lines taking account of linear polarization produced by resonance scattering in lines. Recently, Sampoorna (2012) derived the RM for polarized scattering in subordinate lines taking into account an exact treatment of collisions. This RM is used in the present paper to perform radiative transfer computations. We consider both angle-averaged and azimuth-averaged versions of this RM. Both the angle-averaged and azimuth-averaged type-V redistribution functions are studied in some detail. In the special case of one-dimensional line transfer with axisymmetric conditions, the azimuth-averaged functions indeed represent fully angle-dependent PRD problem. We compare the Stokes profiles computed using angle-averaged and azimuth-averaged RM, and show that it is good enough to use angle-averaged functions in practical applications. However, in multi-dimensional polarized line transfer, the kind of azimuthal averaging used in this paper is no longer valid due to symmetry breaking. A decomposition method for such interesting situations are discussed in Anusha & Nagendra (2011, 2012) for the case of resonance lines. It can be extended to the case of subordinate lines also.

We have devised a polarized approximate lambda iteration method to solve the subordinate line transfer equation in a one-dimensional planar medium. To compute the line source vector corrections, we present two alternative methods. The first one is a matrix method (called the frequency-by-frequency method for angle-averaged case; and the frequency-angle by frequency-angle method for azimuth-averaged case), which is computationally slow. The second one is a faster method and is similar to the well-known core–wing separation method of Paletou & Auer (1995) for resonance lines. This method, in the case of subordinate lines, is applicable when the lower level damping width is smaller than the upper level damping width. When the lower level damping width is comparable or larger than that of the upper level, we show that a method similar to the CRDA method of Scharmer (1983) becomes applicable (whereas this method does not work well for resonance lines, it poses no difficulty in the case of subordinate lines).

Our numerical experiments show that the type-V redistribution cannot simply be replaced by CRD function, particularly when treating scattering polarization of subordinate lines. The linear polarization profiles computed by the type-V function lies in between those computed using type-II function and CRD, especially in the line wings. This has direct consequences in polarized spectral diagnostics using subordinate lines (namely, the exact type-V function needs to be used without approximating it either by type-II or CRD functions).

As the relative value of lower level damping parameter with respect to the upper level damping parameter increases, the linear polarization decreases, especially in the line wings. In this way the type-V function becomes more and more frequency non-coherent (similar to CRD) because of which the Q/I profile approaches that computed with CRD. This is in contrast to an increase in the value of the upper level damping parameter, wherein the Q/I profile computed using the type-V function approaches that computed using the type-II function.

Elastic collisions in the upper level produce the same kind of effects for both resonance and subordinate lines. However, they do not affect the lower level as we have assumed it to be unpolarized.

We are grateful to the referee for critical comments which helped to qualitatively improve the paper. We thank Dr. V. Bommier for providing the programs to compute the Gauss–Legendre angle quadratures and the angle-dependent type-III function.

REFERENCES

Adams, T. F., Hummer, D. G., & Rybicki, G. B. 1971, J. Quant. Spectrosc. Radiat. Transfer, 11, 1365
Anusha, L. S., & Nagendra, K. N. 2011, ApJ, 739, 40
Anusha, L. S., & Nagendra, K. N. 2012, ApJ, 746, 84
Bommier, V. 1997a, A&A, 328, 706
Bommier, V. 1997b, A&A, 328, 726
Domke, H., & Hubeny, I. 1988, ApJ, 334, 527
Faurobert, M. 1987, A&A, 178, 269
Frisch, H. 1980, A&A, 87, 357
Frisch, H. 2010, A&A, 522, A41
Heinzel, P. 1981, J. Quant. Spectrosc. Radiat. Transfer, 25, 483
Heinzel, P., & Hubeny, I. 1982, J. Quant. Spectrosc. Radiat. Transfer, 27, 1
Heinzel, P., & Hubeny, I. 1983, J. Quant. Spectrosc. Radiat. Transfer, 30, 77
Hubeny, I. 1985, A&A, 145, 461
Hubeny, I., & Heinzel, P. 1984, J. Quant. Spectrosc. Radiat. Transfer, 32, 159
Hummer, D. G. 1962, MNRAS, 125, 21
McKenna, S. J. 1984, Ap&SS, 106, 283

Mohan Rao, D., Rangarajan, K. E., & Peraiah, A. 1984, JA&A, 5, 169
Nagendra, K. N. 1994, ApJ, 432, 274
Nagendra, K. N. 1995, MNRAS, 274, 523
Nagendra, K. N. 2003, in ASP Conf. Ser. 288, Stellar Atmosphere Modeling, ed. I. Hubeny, D. Mihalas, & K. Werner (San Francisco, CA: ASP), 583
Nagendra, K. N., Frisch, H., & Faurobert, M. 2002, A&A, 395, 305
Nagendra, K. N., & Sampoorna, M. 2009, in ASP Conf. Ser. 405, Solar Polarization 5, ed. S. V. Berdyugina, K. N. Nagendra, & R. Ramelli (San Francisco, CA: ASP), 261
Nagendra, K. N., & Sampoorna, M. 2011, A&A, 535, A88
Omont, A., Smith, E. W., & Cooper, J. 1972, ApJ, 175, 185
Paletou, F., & Auer, L. H. 1995, A&A, 297, 771
Rees, D. E., & Saliba, G. J. 1982, A&A, 115, 1
Sampoorna, M. 2012, ApJ, 745, 189
Sampoorna, M., Nagendra, K. N., & Frisch, H. 2008, J. Quant. Spectrosc. Radiat. Transfer, 109, 2349
Sampoorna, M., Nagendra, K. N., & Frisch, H. 2011, A&A, 527, A89
Scharmer, G. B. 1983, A&A, 117, 83
Stenflo, J. O. 1994, Solar Magnetic Fields : Polarized Radiation Diagnostics (Dordrecht: Kluwer)
Trujillo Bueno, J. 2003, in ASP Conf. Ser. 288, Stellar Atmosphere Modeling, ed. I. Hubeny, D. Mihalas, & K. Werner (San Francisco, CA: ASP), 551